Stringent Constraints on New Pseudoscalar and Vector Bosons from Precision Hyperfine Splitting Measurements

Cedric Quint,[1] Fabian Heiße,[1] Joerg Jaeckel,[2] Lutz Leimenstoll,[2] Christoph H. Keitel,[1] and Zoltán Harman[1]
[1]Max Planck Institute for Nuclear Physics, Saupfercheckweg 1, 69117 Heidelberg, Germany
[2]Institute for Theoretical Physics, Philosophenweg 16, 69120 Heidelberg, Germany

(Received 12 June 2025; revised 28 October 2025; accepted 20 February 2026; published 19 March 2026)

Axionlike particles and similar new pseudoscalar as well as vector bosons coupled to nucleons and electrons are predicted to lead to spin-dependent forces in atoms and ions. We argue that hyperfine structure measurements in hydrogenlike and lithiumlike charge states are a sensitive probe to this effect. Employing specific differences of these splittings reduces uncertainties due to nuclear effects in hyperfine structure calculations and measurements. Using this, we show that existing measurements on Be provide competitive limits in the region $m_\phi \gtrsim 100$ keV, confirming, or improving by up to a factor of 2, existing constraints for pseudoscalar couplings, depending on the nuclear model. We also find that future measurements on Cs have a further factor of 2-2.5 improved discovery potential for pseudoscalars and an order of magnitude for new vector bosons when compared with the corresponding current constraints.

DOI: 10.1103/rvt1-93v2

In recent years, there has been increasing interest in investigating physics beyond the standard model (SM) using the tools of precision atomic spectroscopy (cf. Refs. [1–11]) as well as similar approaches (cf. Refs. [12–18]). Notably, a recent review [19] highlighted the sensitivity of atomic systems to new physics-induced spin-dependent interactions. This motivates new physics searches based on the prediction that the exchange of new bosons also implies the existence of new forces and potentials [20,21].

Most existing constraints focus on light atoms or isotope shifts, where theoretical and experimental precision exceeds that of heavier-element spectroscopy [5,15]. We argue that highly charged ions can also play an important role, notably for pseudoscalars and vector bosons.

Generally speaking, the experimental approach best suited for investigating forces induced by new particles depends on the Lorentz structure of the interaction [20,21]. In this Letter, we focus on pseudoscalar and vector interactions, leading to a dipole-dipole interaction between the electron(s) and the nucleus.

Pseudoscalars appear in a wide range of extensions to the SM. Light variants with interactions that are suppressed by a large new physics scale are often called axions or axionlike particles [22–25]. This is motivated by their similarity to QCD axions that arise as a consequence of the Peccei-Quinn solution to the strong charge parity problem in QCD [26–31] (see Ref. [32] for an overview of models). In field theory, such pseudoscalars arise as pseudo Nambu-Goldstone bosons of a spontaneously broken global symmetry. They can also arise in string theory scenarios [33–46]. Similarly, extra vector bosons can be viewed as one of the simplest extensions of the SM, notably its gauge symmetries by a U(1) factor [47,48]. They can interact directly (see, e.g., Refs. [49–52] for some flavor dependent options) via kinetic mixing [53–55] or higher dimensional operators [21,56], and they, too, are a generic feature of string-based models [57–66].

Both pseudoscalars and light vectors arise in solutions to various open problems in physics, most notably as a possible light dark matter candidate [37,67–73].

Because of their Lorentz structure, interactions mediated by such particles induce spin-spin couplings in atomic systems [20,21]. Hence, they give rise to an additional contribution to the hyperfine splitting (HFS) in such systems, thereby giving access to possible experimental signatures.

For higher masses, such interactions are expected to be short ranged, making them harder to detect in fifth force experiments, and limits are typically weaker [19]. To access the $\sim$(1–100) MeV range, choosing an element with a high nuclear charge Z is an intuitive step, resulting in a shorter mean distance between the bound electron and the nucleus. However, finite-nuclear-size-effects (FNS) grow with increasing Z, reducing theoretical precision. We mitigate this by considering specific differences of hyperfine splittings. These are weighted differences between the hyperfine splitting energy of lithiumlike and hydrogenlike ions, with

Published by the American Physical Society under the terms of the Creative Commons Attribution 4.0 International license. Further distribution of this work must maintain attribution to the author(s) and the published article's title, journal citation, and DOI. Funded by SCOAP³.

the weighting factor defined such that the effects due to the magnetization distribution of the nucleus are largely suppressed [74]. The study of HFS in both charge states has recently been enabled by experimental developments with stored and trapped ions in the high-Z [75] and low-Z [76] regimes. This improves HFS bounds on pseudoscalar and vector couplings, even for hydrogen and helium [19,77]. However, this also results in a suppression of the new physics effects for hydrogen and helium. This suppression is less pronounced for medium to highly charged ions (HCI) that can thus yield competitive bounds on those new interactions: as we show below, in the high-mass regime, the bounds can be improved by up to a factor of 2.5 for pseudoscalars and an order of magnitude for vectors compared to the best previous results. Another advantage of HCIs is that, via the choice of the isotope, one can selectively constrain proton and neutron coupling constants [78] opening promising directions for further improvement.

Theory—The hyperfine structure of hydrogen has a rich history in the study of relativistic and radiative corrections to the energy levels predicted by the Schrödinger equation. This field has reached a high level of maturity, enabling remarkable precision in theory and experiment [75,76,79–82]. The development of diverse methods in recent decades has yielded numerous insights into HFS in hydrogenlike and lithiumlike ions. The former can be encapsulated into the following parametrization of the ground-state HFS of hydrogenlike ions [79]:

$$\triangle E_{\text{H-like}} = \frac{4}{3}\alpha(\alpha Z)^3 \frac{\mu}{\mu_N}\frac{m_e}{m_p}\frac{2I+1}{2I}\frac{m_e}{\left(1+\frac{m_e}{M}\right)^3} \times [A_{1s}(\alpha Z)(1-\delta_{1s})(1-\varepsilon_{1s}) + x^{1s}_{\text{rad}}]. \quad (1)$$

Here, α is the fine-structure constant, Z the nuclear charge, m_e (m_p) the electron (proton) mass, V the nuclear magnetic moment (magneton), I the nuclear spin, and M the nuclear mass. We use natural units ($\hbar = c = 1$). The factor $A_{1s}(\alpha Z)$ denotes the relativistic correction [83]. Furthermore, δ_{1s} is the nuclear charge distribution correction, and ε_{1s} is the nuclear magnetization distribution correction [Bohr-Weisskopf (BW) correction]. Finally, x^{1s}_{rad} denotes radiative corrections ([79,84,85]).

For lithiumlike ions, one can observe a similar structure in HFS contributions, with the addition of interelectronic interaction contributions [79],

$$\triangle E_{\text{Li-like}} = \frac{1}{6}\alpha(\alpha Z)^3 \frac{\mu}{\mu_N}\frac{m_e}{m_p}\frac{2I+1}{2I}\frac{m_e}{\left(1+\frac{m_e}{M}\right)^3} \times \left(\left[A_{1s}(\alpha Z) + \frac{1}{Z}B(\alpha Z) + \ldots\right] \times (1-\delta_{2s})(1-\varepsilon_{2s}) + x^{2s}_{\text{rad}}\right). \quad (2)$$

Here, $A_{2s}(\alpha Z)$ denotes the relativistic factor for the $2s$ system, $B(\alpha Z)$ denotes the photon exchange contribution to first order, and x^{2s}_{rad} parametrizes the radiative corrections for the lithiumlike system. Moreover, δ_{2s} and ε_{2s} again denote the nuclear charge distribution and BW correction, respectively. We note that the photon exchange contributions admit a $1/Z$ expansion, since each exchange provides a factor α in the $Z\alpha$ expansion. We calculate the energy shift induced by the spin-dependent interaction between an electron and the nucleus. To model nuclear couplings of new particles, we use the single-particle Schmidt model [86]. Here, the spin of a nucleus with an odd number of nucleons arises from the total angular momentum of the valence nucleon. All other nucleons do not contribute to the spin-dependent coupling. Hence, the electron effectively couples to that valence nucleon only [86,87]. We therefore interpret the interaction as a coupling to the dipole operator $\boldsymbol{\mu}_N = g_I^{\text{NP}}\boldsymbol{I}$, where g_I^{NP} is the new physics associated the nuclear g factor evaluated using nuclear shell states. Although reasonably well justified, this assumption could be improved upon [88]. We account for the introduced error by adopting conservative constraints based on the nuclear model comparison in Ref. [88] (see the End Matter for details).

We represent the corresponding interaction Lagrangian as

$$\mathcal{L}_{\text{int}} = \sum_{k=e,N} i g_k \bar{\psi}_k \gamma^5 \psi_k \phi + y_k \bar{\psi}_k \gamma^\mu \psi_k Z_\mu. \quad (3)$$

Here, ψ_k denotes the Dirac field of the electron e or nucleon $N \in \{n, p\}$, where n denotes the neutron and p is the proton. Moreover, g_k/y_k is the respective coupling constant of the pseudoscalar/vector field to the indexed particle, ϕ/Z_μ is the pseudoscalar/vector field, and γ^5/γ^μ denote the Dirac gamma matrices. Using the nonrelativistic approximation for the dynamics of the nucleons, one obtains the following potential from the aforementioned interaction Lagrangian [77,89]:

$$V_{\phi/Z}(r) = \frac{g_N g_e}{8\pi m_N}\boldsymbol{\mu}_N \cdot \boldsymbol{T}\frac{e^{-m_{\phi/Z}r}}{r}(m_{\phi/Z} + 1/r), \quad \boldsymbol{T} = \begin{cases} i\hat{\boldsymbol{r}}\gamma^0\gamma^5, & \text{Pseudoscalar}, \\ \hat{\boldsymbol{r}} \times \gamma^0\boldsymbol{\gamma}, & \text{Vector}. \end{cases} \quad (4)$$

Here, r is the radial variable in the system of the nucleus; $\boldsymbol{\mu}_N$ is the aforementioned dipole operator as described in the End Matter; m_N and $m_{\phi/Z}$ are the masses of the nucleon and the exchange boson, respectively; and $\hat{\boldsymbol{r}} = \boldsymbol{r}/r$ is the unit coordinate vector.

Using the Wigner–Eckart theorem [90], we obtain the induced HFS,

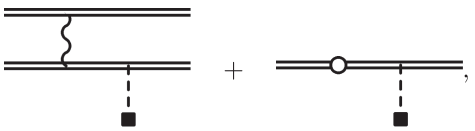
$$\triangle E = g_I^{\mathrm{NP}} \frac{g_N g_e}{4\pi} \frac{m_e^2}{2m_N} \frac{(2I+1)}{\sqrt{6}} \times \int_r \psi^{\dagger}_{n,\kappa,m}(\boldsymbol{r})(\beta(r)\boldsymbol{T})\psi_{n,\kappa,m}(\boldsymbol{r})\mathrm{d}\boldsymbol{r}. \quad (5)$$

Here, κ is the relativistic angular momentum quantum number of the electron. The functions $\psi_{n,\kappa,m}$ called Dirac-Coulomb wave functions are obtained in the nuclear potential corresponding to the Fermi proton distribution (see Refs. [90,91] and the End Matter). Moreover, we defined the potential function as

$$\beta(r) = \frac{e^{-m_\phi r}}{r}(m_\phi + 1/r). \quad (6)$$

From this, the new physics induced hyperfine structure becomes readily calculable in one electron systems. For lithiumlike ions, however, interelectronic interactions become relevant due to the overlap of the core and valence s electrons in the nuclear region. We treat this effect as discussed in [82], i.e., via the addition of screening terms to the nuclear potential and perturbation theory in α. The former is known as treating the system within the *extended Furry picture* [82,92,93]. To this end, we take the effective potential for the electrons in the lithiumlike system to be the Kohn-Sham (KS) potential [94,95] from density functional theory [93,96], as explicitly given in the End Matter. The KS potential is determined by the electron probability density around the nucleus, which we obtain self-consistently from Dirac-Hartree-Fock (DHF) wave functions [97]. The hyperfine structure calculations are then carried out using radial wave functions that were obtained by solving the Dirac equation with this modified potential term.

Up to the first order in α, we consider the one photon exchange contribution to the HFS in the lithiumlike system perturbatively. Schematically, this contribution is given by the following diagram:



(7)

where a double line denotes an electron propagating in the screened nuclear potential V, the wavy line represents the exchange of a photon, and the dashed line terminated by a square is the pseudoscalar or vector potential $V_{\phi/Z}$ in Eq. (4). The second diagram denotes a counterterm contribution that we add to avoid double-counting interaction effects when calculating the photon exchange contribution within the extended Furry picture. Hence, the white circle denotes an insertion of the screening potential. For details on this calculation, see Supplemental Material, End Matter, and Ref. [82].

With this approach, we have included Coulomb interactions between electrons to high order by using a self-consistent screening potential and included relativistic corrections up to the first order by including photon exchange.

We derive constraints from the *specific difference* of HFS energies between lithiumlike and hydrogenlike ions of the same isotope. This weighted difference is constructed to suppress uncertainties originating from the BW effect [98].

These specific differences were first discussed for bismuth in Ref. [74] and can be calculated with significantly higher precision than the individual HFS contributions. They are defined as

$$\triangle' E = \triangle E_{\text{Li-like}} - \xi \triangle E_{\text{H-like}}. \quad (8)$$

Here, the factor ξ is the ratio of the BW shifts, i.e.,

$$\xi = \frac{\triangle E^{\mathrm{BW}}_{\text{Li-like}}}{\triangle E^{\mathrm{BW}}_{\text{H-like}}}. \quad (9)$$

Since ξ can be determined more precisely than individual BW terms, the specific difference yields a robust observable with reduced uncertainty. Note that ξ is fully determined within the SM and FNS effects enter only as small corrections to the new physics contribution. We have ensured that this is a small effect.

For many elements, tabulated values of ξ are unavailable. In these cases, we extract ξ from the BW shifts in Ref. [99]. Where available, we use dedicated calculations of ξ. Our bounds are insensitive to variations in ξ beyond the fourth digit.

We compare with constraints from hydrogen and helium. For these elements, an alternative specific difference D_{21} can be defined [1]. It compares the HFS of a $1s$ and excited $2s$ state

$$D_{21} = 8\triangle E_{2s} - \triangle E_{1s}, \quad (10)$$

where $\triangle E_{1s}$ is the $1s$ HFS and $\triangle E_{2s}$ corresponds to the respective $2s$ HFS. This is analogous to $\triangle' E$ with $\xi = 1/8$, which approximately holds for low-Z elements. In Table I, we present the theory and experimental values for D_{21} in helium and hydrogen along with the values for $\triangle' E$ in heavier elements. Details on the experimental and theoretical precision are given in Supplemental Material [100].

Results—We follow an approach similar to Ref. [114], determining the 95% confidence interval (CI) for the difference between theory and experiment. The Gaussian parameters are

$$\bar{x} = |\text{Theory} - \text{Experiment}|$$
$$\sigma = \sqrt{\sigma^2_{\text{theo}} + \sigma^2_{\text{exp}}}. \quad (11)$$

TABLE I. Values for ξ, I, g_I^{NP}, and specific differences (D_{21} for helium and hydrogen, $\triangle' E$ for the rest) for different elements. TW indicates uncertainty estimates derived in this Letter (see Supplemental Material [100]).

Element	I	$\lvert g_I^{\mathrm{NP}}\rvert$		ξ	Theory (meV)	Experiment (meV)	Refs.
		Pseudosc.	Vector				
^{1}H	1/2	2	2	0.125	$2.02458(10)\times10^{-7}$	$2.02479(28)\times10^{-7}$	[114]
^{3}He	1/2	2	2	0.125	$-4.9218(6)\times10^{-6}$	$-4.92136(29)\times10^{-6}$	[115]
^{9}Be	3/2	2/3	4/3	0.04881891046	$-1.224(15)\times10^{-6}$	$-1.13581526(5)\times10^{-6}$	[76]
^{131}Xe	3/2	2/5	4/5	0.13660	$\triangle' E_{\mathrm{Xe}}\pm7\times10^{-5}$	$\triangle' E_{\mathrm{Xe}}\pm1\times10^{-5}$	[99], TW
^{133}Cs	7/2	2/9	8/9	0.13745	$\triangle' E_{\mathrm{Cs}}\pm7\times10^{-5}$	$\triangle' E_{\mathrm{Cs}}\pm1\times10^{-5}$	[99], TW
^{209}Bi	9/2	2/9	10/9	0.16885	$-61.043(35)$	$-61.012(26)$	[74,75]

To set our constraints we use the 95% CI bound $\delta E = \delta' E + \bar{x}$, with $\delta' E$ defined by

$$95\% = \frac{1}{\sqrt{2\pi\sigma}} \int_{-\delta' E+\bar{x}}^{\delta' E+\bar{x}} e^{\frac{-(x-\bar{x})^2}{2\sigma}} \mathrm{d}x, \tag{12}$$

yielding conservative bounds. For caesium and xenon projections we set $\bar{x} = 0$ and use estimated uncertainties. Bounds then follow from

$$|\triangle E_{\text{Li-like}} - \xi \triangle E_{\text{H-like}}| \leq \delta E. \tag{13}$$

We also include possible new-boson contributions to the nuclear g factor in the corresponding measurement via the Zeeman splitting of hyperfine levels [116,117]. Since the HFS and the nuclear g-factor measurement form a nondegenerate system, the two can be disentangled. This is outlined in the End Matter. We find that taking this into account reproduces the constraints derived from Eq. (13), shown in Fig. 1.

Future Cs measurements promise to extend the sensitivity to the electron–proton couplings, by up to a factor of 2-2.5 for pseudoscalars and an order of magnitude for vectors for higher masses; see Supplemental Material for the discussion regarding required uncertainties of theory and experiment [100]. Using Be already matches or improves the sensitivity to pseudoscalar couplings with neutrons by up to a factor of 2, depending on the nuclear model. These constraints supersede astrophysical exclusions in Ref. [19], which stop at $m_\phi \gtrsim 10^4$ eV. We note the expected feature that heavier elements provide better bounds at higher masses due to the lower mean distance between the electrons and the nucleus. However, this is tempered by reduced theoretical and experimental precision. At low masses, differences between bounds cannot be attributed to sensitivities alone. We also find that the strength of the constraint depends on the scaling of the specific difference, i.e., if the specific difference due to new physics scales similarly to the BW effect, the resulting bounds are less stringent. This occurs for hydrogen and helium, where the scaling is almost identical. This is the suppression that we mentioned in the introduction, indicating that heavier elements can indeed be better suited to derive such constraints despite the reduced sensitivities due to nuclear effects.

Said suppression can be attributed to the systems used to form the specific differences in helium and hydrogen not including interelectronic interactions, which enables us to consider the following ratio:

$$\frac{\int \mathrm{d}r F_{2s}(r) G_{2s}(r) \beta(r)}{\int \mathrm{d}r F_{1s}(r) G_{1s}(r) \beta(r)} \overset{m_\phi \to 0}{\to} \frac{1}{8} + \mathcal{O}((Z\alpha)^2), \tag{14}$$

implying (note that $\xi = 1/8$ for helium and hydrogen) that the new physics contributions in the hydrogen and helium specific differences cancel for low masses up to relativistic corrections. Note that this may also happen for heavier elements depending on the value of ξ. However, this is not the case for the systems that we consider, for which we found that the missing suppression is not caused by computational inaccuracies.

We note that astrophysical constraints on the electron coupling can be extended to higher masses using results from Ref. [122]. However, the corresponding supernova bound on nucleons likely falls into the trapping regime, weakening the constraint (cf. Ref. [123]).

Conclusion—We derive bounds on new light bosons from hyperfine splittings in highly charged ions. We employ specific differences, which largely overcome theoretical limitations from the Bohr–Weisskopf effect. This demonstrates that future precision spectroscopy of mid- to high-Z ions can yield competitive bounds on the pseudoscalar and vector couplings, improving upon constraints from hydrogen and helium by up to a factor of 2 and an order of magnitude, respectively.

This analysis of new physics induced atomic interactions can be extended beyond our Letter by considering additional interaction types and higher-order QED contributions.

Acknowledgments—C. Q. wishes to thank V. A. Yerokhin, N. S. Oreshkina, and L. Pütter for insightful discussions. This work is supported by the Collaborative Research Centre 1225 funded by Deutsche

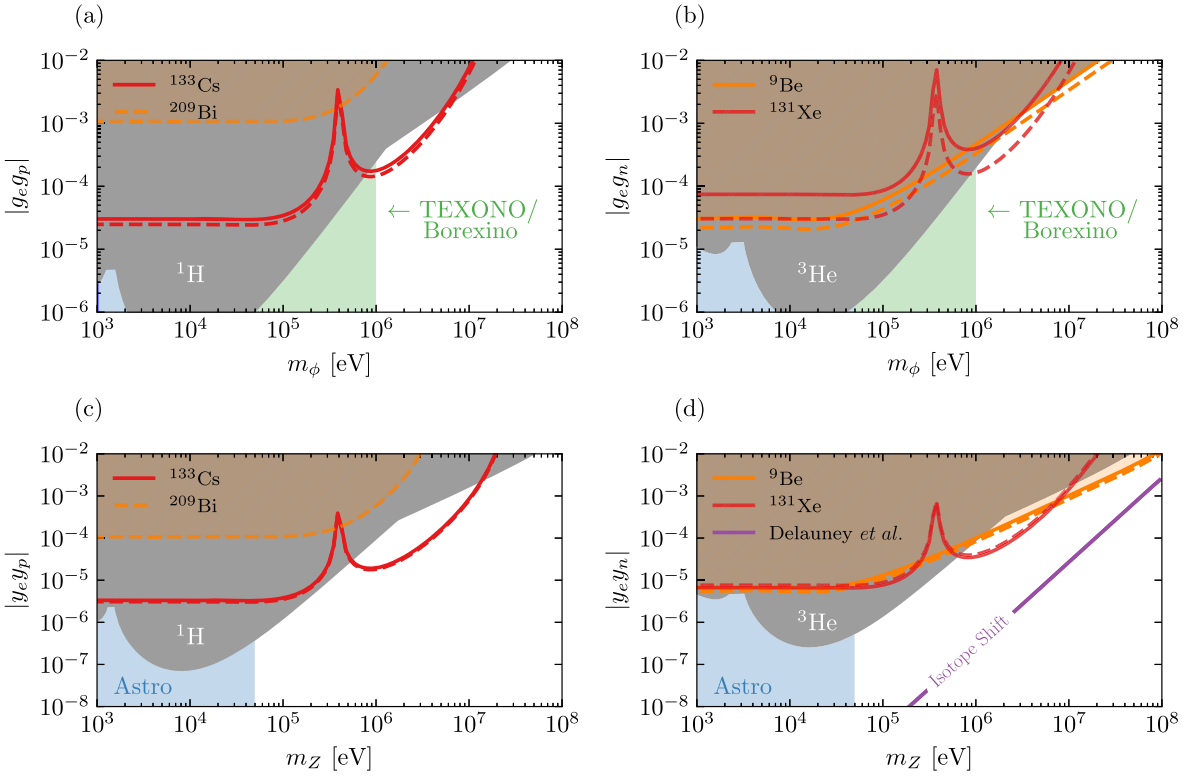


FIG. 1. Bounds on the pseudoscalar (top) and vector (bottom) parameter space. (a),(c) Bounds on the product of the electron and proton couplings and (b),(d) bounds on the product of electron and neutron couplings. Red lines (projections) and orange regions (current constraints) are derived in this Letter. The gray area on the left denotes bounds from the hydrogen specific difference D_{21}^{H} [114] and $1s$ HFS [118]. The gray area on the right side denotes bounds from the helium-3 specific difference D_{21}^{He} and $1s$ HFS. In the vector electron–neutron case, isotope-shift constraints are shown in purple [19,119]. Green shows TEXONO [120] and Borexino [121] constraints; blue denotes astrophysical constraints [19]. Solid lines show conservative bounds accounting for estimated uncertainties (see Supplemental Material [100]) and possible Schmidt-model errors [88]. Dashed lines indicate Schmidt model results. The bismuth constraint is a projection assuming that a direct measurement of the magnetic moment will agree with the nuclear magnetic resonance (NMR) result. The regions appearing as brown within our plot indicate our results (orange) overlapping with the hydrogen and helium constraints (gray).

Forschungsgemeinschaft (DFG, German Research Foundation) Project No. 273811115–SFB 1225 ISOQUANT. This article comprises parts of the PhD thesis work of C. Q. to be submitted to Heidelberg University.

Data availability—The data that support the findings of this article are not publicly available. The data are available from the authors upon reasonable request.

[1] S. G. Karshenboim and V. G. Ivanov, Phys. Lett. B **524**, 259 (2002).
[2] J. Jaeckel and S. Roy, Phys. Rev. D **82**, 125020 (2010).
[3] S. G. Karshenboim, Phys. Rev. D **82**, 113013 (2010).
[4] F. Ficek, D. F. J. Kimball, M. G. Kozlov, N. Leefer, S. Pustelny, and D. Budker, Phys. Rev. A **95**, 032505 (2017).
[5] V. Debierre, C. H. Keitel, and Z. Harman, Phys. Lett. B **807**, 135527 (2020).
[6] G. Adkins, D. Cassidy, and J. Pérez-Ríos, Phys. Rep. **975**, 1 (2022).
[7] T. Sailer, V. Debierre, Z. Harman, F. Heiße, C. König, J. Morgner, B. Tu, A. V. Volotka, C. H. Keitel, K. Blaum, and S. Sturm, Nature (London) **606**, 479 (2022).
[8] R. M. Potvliege, New J. Phys. **27**, 045002 (2025).
[9] M. Door *et al.*, Phys. Rev. Lett. **134**, 063002 (2025).
[10] L. Cong, F. Ficek, P. Fadeev, Y. V. Stadnik, and D. Budker, arXiv:2503.07161.
[11] R. M. Potvliege, A. Nicolson, M. P. A. Jones, and M. Spannowsky, Phys. Rev. A **108**, 052825 (2023).
[12] K. Wei, W. Ji, C. Fu, A. Wickenbrock, J. Fang, V. V. Flambaum, and D. Budker, Nat. Commun. **13**, 7387 (2022).
[13] W. Ji, W. Li, P. Fadeev, F. Ficek, J. Qin, K. Wei, Y.-C. Liu, and D. Budker, Phys. Rev. Lett. **130**, 133202 (2023).
[14] K. A. Beyer, I. A. Valuev, C. H. Keitel, M. Tamburini, and N. S. Oreshkina, Phys. Lett. B **854**, 138746 (2024).
[15] A. Wilzewski *et al.*, Phys. Rev. Lett. **134**, 233002 (2025).
[16] Z. Xu, X. Heng, G. Tian, D. Gong, L. Cong, W. Ji, D. Budker, and K. Wei, Phys. Rev. Lett. **134**, 181801 (2025).
[17] B. Elder, G. Mentasti, E. Pasatembou, C. F. A. Baynham, O. Buchmueller, C. R. Contaldi, C. de Rham, R. Hobson, and A. J. Tolley, Phys. Rev. D **112**, 044053 (2025).

[18] J. W. D. Halliday *et al.*, Phys. Rev. Lett. **134**, 055001 (2025).
[19] L. Cong *et al.*, Rev. Mod. Phys. **97**, 025005 (2025).
[20] J. E. Moody and F. Wilczek, Phys. Rev. D **30**, 130 (1984).
[21] B. A. Dobrescu and I. Mocioiu, J. High Energy Phys. 11 (2006) 005.
[22] J. E. Kim, Phys. Rep. **150**, 1 (1987).
[23] J. Jaeckel and A. Ringwald, Annu. Rev. Nucl. Part. Sci. **60**, 405 (2010).
[24] J. Beacham *et al.*, J. Phys. G **47**, 010501 (2020).
[25] P. Agrawal *et al.*, Eur. Phys. J. C **81**, 1015 (2021).
[26] R. D. Peccei and H. R. Quinn, Phys. Rev. Lett. **38**, 1440 (1977).
[27] S. Weinberg, Phys. Rev. Lett. **40**, 223 (1978).
[28] J. E. Kim, Phys. Rev. Lett. **43**, 103 (1979).
[29] M. A. Shifman, A. I. Vainshtein, and V. I. Zakharov, Nucl. Phys. **B166**, 493 (1980).
[30] A. R. Zhitnitsky, Sov. J. Nucl. Phys. **31**, 260 (1980).
[31] M. Dine, W. Fischler, and M. Srednicki, Phys. Lett. **104B**, 199 (1981).
[32] L. Di Luzio, M. Giannotti, E. Nardi, and L. Visinelli, Phys. Rep. **870**, 1 (2020).
[33] J. P. Conlon, J. High Energy Phys. 05 (2006) 078.
[34] J. P. Conlon, Phys. Rev. Lett. **97**, 261802 (2006).
[35] A. Arvanitaki, S. Dimopoulos, S. Dubovsky, N. Kaloper, and J. March-Russell, Phys. Rev. D **81**, 123530 (2010).
[36] M. Cicoli, M. Goodsell, and A. Ringwald, J. High Energy Phys. 10 (2012) 146.
[37] D. J. E. Marsh, Phys. Rep. **643**, 1 (2016).
[38] B. S. Acharya and C. Pongkitivanichkul, J. High Energy Phys. 04 (2016) 009.
[39] L. Visinelli and S. Vagnozzi, Phys. Rev. D **99**, 063517 (2019).
[40] I. Broeckel, M. Cicoli, A. Maharana, K. Singh, and K. Sinha, J. High Energy Phys. 08 (2021) 059.
[41] M. Demirtas, N. Gendler, C. Long, L. McAllister, and J. Moritz, J. High Energy Phys. 06 (2023) 092.
[42] V. M. Mehta, M. Demirtas, C. Long, D. J. E. Marsh, L. McAllister, and M. J. Stott, J. Cosmol. Astropart. Phys. 07 (2021) 033.
[43] N. Gendler, D. J. E. Marsh, L. McAllister, and J. Moritz, J. Cosmol. Astropart. Phys. 09 (2024) 071.
[44] N. Gendler and D. J. E. Marsh, Phys. Rev. Lett. **134**, 081602 (2025).
[45] R. Petrossian-Byrne and G. Villadoro, J. High Energy Phys. 07 (2025) 049.
[46] V. Loladze, A. Platschorre, and M. Reig, J. High Energy Phys. 08 (2025) 182.
[47] J. Jaeckel, Frascati Phys. Ser. **56**, 172 (2012).
[48] M. Fabbrichesi, E. Gabrielli, and G. Lanfranchi, The dark photon, *SpringerBriefs in Physics* (Springer, New York, 2020).
[49] X. G. He, G. C. Joshi, H. Lew, and R. R. Volkas, Phys. Rev. D **43**, 22 (1991).
[50] X.-G. He, G. C. Joshi, H. Lew, and R. R. Volkas, Phys. Rev. D **44**, 2118 (1991).
[51] J. Heeck and W. Rodejohann, Phys. Rev. D **84**, 075007 (2011).
[52] M. Bauer, P. Foldenauer, and J. Jaeckel, J. High Energy Phys. 07 (2018) 094.
[53] L. B. Okun, Sov. Phys. JETP **56**, 502 (1982).
[54] B. Holdom, Phys. Lett. **166B**, 196 (1986).
[55] R. Foot and X.-G. He, Phys. Lett. B **267**, 509 (1991).
[56] B. A. Dobrescu, Phys. Rev. Lett. **94**, 151802 (2005).
[57] M. Goodsell, in *Proceedings of the 5th Patras Workshop on Axions, WIMPs and WISPs* (DESY, Hamburg, Germany, 2009), pp. 165–168.
[58] M. Goodsell, J. Jaeckel, J. Redondo, and A. Ringwald, J. High Energy Phys. 11 (2009) 027.
[59] M. Bullimore, J. P. Conlon, and L. T. Witkowski, J. High Energy Phys. 11 (2010) 142.
[60] M. Cicoli, M. Goodsell, J. Jaeckel, and A. Ringwald, J. High Energy Phys. 07 (2011) 114.
[61] P. G. Camara, L. E. Ibanez, and F. Marchesano, J. High Energy Phys. 09 (2011) 110.
[62] F. Marchesano, D. Regalado, and G. Zoccarato, J. High Energy Phys. 08 (2014) 157.
[63] P. Anastasopoulos, M. Bianchi, D. Consoli, and E. Kiritsis, Fortschr. Phys. **69**, 2100034 (2021).
[64] A. Hebecker, J. Jaeckel, and R. Kuespert, J. High Energy Phys. 04 (2024) 116.
[65] E. Sheridan, F. Carta, N. Gendler, M. Jain, D. J. E. Marsh, L. McAllister, N. Righi, K. K. Rogers, and A. Schachner, J. High Energy Phys. 09 (2025) 016.
[66] T. Coudarchet, A. Hebecker, J. Jaeckel, and J. Steiner, arXiv:2510.12874.
[67] J. Preskill, M. B. Wise, and F. Wilczek, Phys. Lett. **120B**, 127 (1983).
[68] L. F. Abbott and P. Sikivie, Phys. Lett. **120B**, 133 (1983).
[69] M. Dine and W. Fischler, Phys. Lett. **120B**, 137 (1983).
[70] A. E. Nelson and J. Scholtz, Phys. Rev. D **84**, 103501 (2011).
[71] P. Arias, D. Cadamuro, M. Goodsell, J. Jaeckel, J. Redondo, and A. Ringwald, J. Cosmol. Astropart. Phys. 06 (2012) 013.
[72] C. B. Adams *et al.*, arXiv:2203.14923.
[73] D. Antypas *et al.*, arXiv:2203.14915.
[74] V. M. Shabaev, A. N. Artemyev, V. A. Yerokhin, O. M. Zherebtsov, and G. Soff, Phys. Rev. Lett. **86**, 3959 (2001).
[75] J. Ullmann *et al.*, Nat. Commun. **8**, 15484 (2017).
[76] S. Dickopf, B. Sikora, A. Kaiser, M. Müller, S. Ulmer, V. A. Yerokhin, Z. Harman, C. H. Keitel, A. Mooser, and K. Blaum, Nature (London) **632**, 757 (2024).
[77] P. Fadeev, Y. V. Stadnik, F. Ficek, M. G. Kozlov, V. V. Flambaum, and D. Budker, Phys. Rev. A **99**, 022113 (2019).
[78] M. Moretti, C. H. Keitel, and Z. Harman, Phys. Rev. Lett. **136**, 011803 (2026).
[79] V. M. Shabaev, M. B. Shabaeva, and I. I. Tupitsyn, Phys. Rev. A **52**, 3686 (1995).
[80] V. M. Shabaev, M. Tomaselli, T. Kühl, A. N. Artemyev, and V. A. Yerokhin, Phys. Rev. A **56**, 252 (1997).
[81] A. Schneider, B. Sikora, S. Dickopf, M. Müller, N. S. Oreshkina, A. Rischka, I. A. Valuev, S. Ulmer, J. Walz, Z. Harman, C. H. Keitel, A. Mooser, and K. Blaum, Nature (London) **606**, 878 (2022).
[82] V. P. Kosheleva, A. V. Volotka, D. A. Glazov, and S. Fritzsche, Phys. Rev. Res. **2**, 013364 (2020).

[83] G. Breit, Phys. Rev. **35**, 1447 (1930).
[84] D. E. Zwanziger, Phys. Rev. **121**, 1128 (1961).
[85] J. R. Sapirstein, Phys. Rev. Lett. **51**, 985 (1983).
[86] T. Schmidt, Z. Phys. **106**, 358 (1937).
[87] L. Leimenstoll, Constraining new pseudoscalar bosons using atomic spectroscopy, Bachelor's thesis, Heidelberg University, 2024.
[88] D. F. J. Kimball, New J. Phys. **17**, 073008 (2015).
[89] V. A. Dzuba, V. V. Flambaum, I. B. Samsonov, and Y. V. Stadnik, Phys. Rev. D **98**, 035048 (2018).
[90] M. E. Rose and W. H. Furry, Am. J. Phys. **29**, 866 (1961).
[91] G. W. F. Drake, *Springer Handbook of Atomic, Molecular, and Optical Physics* (Springer, New York, 2006).
[92] J. Sapirstein and K. T. Cheng, Phys. Rev. A **63**, 032506 (2001).
[93] N. S. Oreshkina, D. A. Glazov, A. V. Volotka, V. M. Shabaev, I. I. Tupitsyn, and G. Plunien, Phys. Lett. A **372**, 675 (2008).
[94] W. Kohn and L. J. Sham, Phys. Rev. **140**, A1133 (1965).
[95] P. Hohenberg and W. Kohn, Phys. Rev. **136**, B864 (1964).
[96] J. Sapirstein and K. T. Cheng, Phys. Rev. A **67**, 022512 (2003).
[97] W. R. Johnson, *Atomic Structure Theory* (Springer, Berlin, Heidelberg, 2007).
[98] A. Bohr and V. F. Weisskopf, Phys. Rev. **77**, 94 (1950).
[99] S. Boucard and P. Indelicato, Eur. Phys. J. D **8**, 59 (2000).
[100] See Supplemental Material at http://link.aps.org/supplemental/10.1103/rvt1-93v2, for additional derivations, numerical details, and uncertainty estimates, which includes Refs. [101–113].
[101] A. Egl, I. Arapoglou, M. Höcker, K. König, T. Ratajczyk, T. Sailer, B. Tu, A. Weigel, K. Blaum, W. Nörtershäuser, and S. Sturm, Phys. Rev. Lett. **123**, 123001 (2019).
[102] V. M. Shabaev, Phys. Rep. **356**, 119 (2002).
[103] V. M. Shabaev, M. B. Shabaeva, I. I. Tupitsyn, V. A. Yerokhin, A. N. Artemyev, T. Kühl, M. Tomaselli, and O. M. Zherebtsov, Phys. Rev. A **57**, 149 (1998).
[104] J. E. Rosenthal and G. Breit, Phys. Rev. **41**, 459 (1932).
[105] M. F. Crawford and A. L. Schawlow, Phys. Rev. **76**, 1310 (1949).
[106] O. M. Zherebtsov and V. M. Shabaev, Can. J. Phys. **78**, 701 (2000).
[107] A. V. Volotka and G. Plunien, Phys. Rev. Lett. **113**, 023002 (2014).
[108] W. Quint, D. L. Moskovkhin, V. M. Shabaev, and M. Vogel, Phys. Rev. A **78**, 032517 (2008).
[109] F. Herfurth *et al.* (for the HITRAP Collaboration), Phys. Scr. **2015**, 014065 (2015).
[110] M. Vogel *et al.*, Phys. Scr. **2015**, 014066 (2015).
[111] J. Morgner *et al.*, Nature (London) **622**, 53 (2023).
[112] D. L. Moskovkin, N. S. Oreshkina, V. M. Shabaev, T. Beier, G. Plunien, W. Quint, and G. Soff, Phys. Rev. A **70**, 032105 (2004).
[113] L. V. Skripnikov, S. Schmidt, J. Ullmann, C. Geppert, F. Kraus, B. Kresse, W. Nörtershäuser, A. F. Privalov, B. Scheibe, V. M. Shabaev, M. Vogel, and A. V. Volotka, Phys. Rev. Lett. **120**, 093001 (2018).
[114] L. Cong, F. Ficek, P. Fadeev, and D. Budker, Phys. Rev. A **112**, 052824 (2025).
[115] S. G. Karshenboim, Phys. Rep. **422**, 1 (2005).
[116] V. A. Yerokhin, K. Pachucki, Z. Harman, and C. H. Keitel, Phys. Rev. Lett. **107**, 043004 (2011).
[117] V. A. Yerokhin, K. Pachucki, Z. Harman, and C. H. Keitel, Phys. Rev. A **85**, 022512 (2012).
[118] I. Kuzmenko, T. Kuzmenko, Y. Avishai, and Y. B. Band, Phys. Rev. A **108**, 052804 (2023).
[119] C. Delaunay, C. Frugiuele, E. Fuchs, and Y. Soreq, Phys. Rev. D **96**, 115002 (2017).
[120] H. M. Chang, H. T. Wong, M. H. Chou, M. Deniz, H. X. Huang, F. S. Lee, H. B. Li, J. Li, H. Y. Liao, S. T. Lin, V. Singh, S. C. Wu, and B. Xin, Phys. Rev. D **75**, 052004 (2007).
[121] D. Basilico *et al.* (BOREXINO Collaboration), Eur. Phys. J. C **85**, 1182 (2025).
[122] P. Carenza and G. Lucente, Phys. Rev. D **103**, 123024 (2021).
[123] A. Lella, P. Carenza, G. Co', G. Lucente, M. Giannotti, A. Mirizzi, and T. Rauscher, Phys. Rev. D **109**, 023001 (2024).
[124] W. R. Johnson and G. Soff, At. Data Nucl. Data Tables **33**, 405 (1985).
[125] The distance between the magnetic field source and the ion is large compared with the range of the NP potential, $1/m_{\phi/Z}$, relevant for our constraints. Thus, we can neglect the effect that new bosons may have on this potential.

End Matter

Considered systems, Hamiltonians, and electron wave functions—We consider two different systems to obtain our bounds. The first system is the hydrogenlike ion, for which we use the following Hamiltonian:

$$H_{\text{H-like}} = \boldsymbol{\alpha}\cdot\boldsymbol{p} + \beta m_e + V_{\text{C}}(r), \tag{A1}$$

where α^1, α^2, α^3, and β denote the corresponding Dirac matrices in the Dirac basis and V_{C} accounts for the Coulomb interaction. We model the Coulomb interaction as originating from a Fermi charge distribution [97,124], i.e.,

$$\rho_{\text{C}}(r) = \frac{\rho_0}{1 - e^{\frac{r-c}{a}}}, \tag{A2}$$

where c is the half-density radius and a can be given via the *skin-thickness* t as $a = 4\ln 3 \cdot t$. This yields a constant value for a regardless of the element under consideration. The Hamiltonian for the lithiumlike system is defined analogously as

$$H_{\text{Li-like}} = \boldsymbol{\alpha}\cdot\boldsymbol{p} + \beta m_e + V(r). \tag{A3}$$

Here, $V(r) = V_{\mathrm{KS}}(r) + V_{\mathrm{C}}(r)$ includes screening effects via the Kohn-Sham potential,

$$V_{\mathrm{KS}}(r) = \alpha \int \frac{\rho(r')}{r_>} \mathrm{d}r' - \frac{2\alpha}{3r}\left(r\rho(r)\frac{31}{82\pi^2}\right)^{1/3}, \quad \text{(A4)}$$

with the probability density ρ encoding the screening effects due to the electrons present in the ion. This density is given by

$$\rho(r) = 2[\tilde{F}_{1s}(r)^2 + \tilde{G}_{1s}(r)^2] + [\tilde{F}_{2s}(r)^2 + \tilde{G}_{2s}(r)^2]. \quad \text{(A5)}$$

Here, the wave functions $\tilde{F}, \tilde{G}$ were obtained self-consistently via the DHF procedure outlined in Ref. [97]. Aside from the aforementioned DHF procedure, the corresponding wave functions are obtained by solving the respective Dirac equations, whose general form is as follows:

$$\psi_{n,\kappa,m}(r) = r^{-1}\begin{pmatrix} G_{n,\kappa}(r)\Omega_{\kappa,m}(\theta,\varphi) \\ iF_{n,\kappa}(r)\Omega_{-\kappa,m}(\theta,\varphi) \end{pmatrix}. \quad \text{(A6)}$$

Here, F and G denote the radial wave functions for different parity states, whereas Ω represents spherical spinors. The quantum number n denotes the usual primary quantum number, $\kappa = \pm(j+1/2)$ is the relativistic angular momentum number, and m indicates the angular momentum projection. More information on these functions and their properties can be found in Ref. [91].

The new-physics induced dipole moment and comparisons with full-scale nuclear simulations—As stated in the main text, the interactions facilitated by the inclusion of new pseudoscalars or vector bosons can be formulated as an interaction with a dipole

$$\boldsymbol{\mu} = g^l \boldsymbol{L} + g^s \boldsymbol{S}, \quad \text{(B1)}$$

where we take $g^s = 2$ within our effective coupling framework and indicate the coupling to the angular momentum as

$$g^l = \begin{cases} 1, \text{Vector} \\ 0, \text{Pseudoscalar} \end{cases}. \quad \text{(B2)}$$

The choice of nuclear model now refers to a choice of states with which we calculate the induced nuclear g_I^{NP} factor. In the Schmidt model, this yields

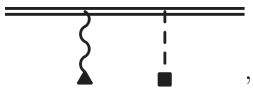
$$g_I^{\mathrm{NP}} = I^{-1}\begin{cases} g^l + \frac{1}{2}g^s, & I = l + \frac{1}{2} \\ \frac{I}{I+1}\left[g^l(l+1) - \frac{1}{2}g^s\right], & I = l - \frac{1}{2} \end{cases}, \quad \text{(B3)}$$

where l is the orbital angular momentum of the valence nucleon. We can also compare with the literature [88] by extracting their values for $\langle \boldsymbol{L} \rangle$ and $\langle \boldsymbol{S} \rangle$. This way, we correct for our overestimating the coupling strength to the valence nucleon to obtain conservative constraints using up-to-date values.

The effect of new physics on the measurement of the nuclear g_I factor—Determination of the standard model value of the specific differences requires the measured nuclear g_I factor as an input. We therefore have to consider the possibility that this measurement, too, is affected by new physics contributions. One possibility to measure the nuclear g_I factor is via a measurement of the g_F factor of a combined system such as a hydrogenlike ion. The nuclear g_I factor can then be extracted via a combined measurement of the Zeeman splitting of two hyperfine states (cf. Refs. [116,117]):

$$\bar{g} = g_{F=I+1/2} + g_{F=I-1/2} = -2\frac{m_e}{m_p} g_I (1-\sigma). \quad \text{(C1)}$$

Here, the dimensionless term σ contains spin-dependent shielding corrections to the bound electron g factor. In the presence of a new boson, there are additional contributions to this quantity, given by the following diagram:



(C2)

where the wavy line terminated by a triangle denotes an insertion of the Zeemann potential induced by an external magnetic field [125],

$$V_{\mathrm{Zee}}(r) = \frac{|e|}{2}\boldsymbol{B}\cdot(\boldsymbol{r}\times\boldsymbol{\alpha}). \quad \text{(C3)}$$

In analogy to the QED case presented in Refs. [116,117], this diagram induces an additional energy shift, given by

$$\begin{aligned} \triangle E = 2\sum_{n\neq a}\sum_{M_I,M_I'}\sum_{M_I'',M_I'''}\sum_{m_a,m_a'}\sum_{m_n,m_n'} & C^{FM_F}_{j_a m_a, IM_I} C^{FM_F}_{j_a m_a', IM_I'} \\ & \times C^{FM_F}_{j_n m_n, IM_I''} C^{FM_F}_{j_n m_n', IM_I'''} \frac{1}{\varepsilon_a - \epsilon_n} \\ & \times \langle IM_I' | \langle a | V_{\mathrm{Zee}} | n \rangle | IM_I'' \rangle \\ & \times \langle IM_I''' | \langle n | V_{\phi/Z} | a \rangle | IM_I \rangle. \end{aligned} \quad \text{(C4)}$$

For the measurements in question, we consider the case $j_a = 1/2$. The nuclear prefactors can then be factored

out, yielding the following expression for the shielding contribution:

$$\sigma_p = \frac{\triangle E}{M_F B \frac{\langle \boldsymbol{I}\cdot\boldsymbol{F}\rangle}{F(F+1)}}, \tag{C5}$$

with the usual angular factor known from hyperfine splitting calculations,

$$\langle \boldsymbol{I}\cdot\boldsymbol{F}\rangle = [F(F+1) - I(I+1) - j(j+1)]/2, \tag{C6}$$

where j denotes the electron spin, I is the nuclear spin, and F stands for the spin of the combined system. From this, we can see that the equation used to determine the nuclear g factor is modified as

$$\bar{g}_p = \bar{g} + 2\frac{m_e}{m_p}\sigma_p. \tag{C7}$$

Similarly, we can write down the SM and new physics contributions to the specific difference of hyperfine splitting intervals. Considering both at the same time, we can connect the variation of both observables with the following system of equations:

$$\begin{pmatrix} \delta(\triangle' E) \\ \delta\bar{g} \end{pmatrix} = \begin{pmatrix} \frac{\partial\triangle' E}{\partial g_I} & \frac{\partial\triangle' E}{\partial g_e g_N} \\ \frac{\partial\bar{g}}{\partial g_I} & \frac{\partial\bar{g}}{\partial g_e g_N} \end{pmatrix} \begin{pmatrix} \delta g_I \\ \delta(g_e g_N) \end{pmatrix}, \tag{C8}$$

where $g_N \in \{g_n, g_p\}$ denotes either the neutron or proton coupling of the pseudoscalar (the treatment is analogous for vector bosons). We find that the matrix in the above equation is invertible within the mass range in which we derive our bounds, meaning we can disentangle the two measurements. Our bounds are then also obtained by solving the above system of equations (see also Ref. [2]), i.e.,

$$|\delta(g_e g_p)| \leq \frac{\left|\frac{\partial\triangle' E}{\partial g_I}\delta\bar{g}\right| + \left|\frac{\partial\bar{g}}{\partial g_I}\delta(\triangle' E)\right|}{\left|\frac{\partial\triangle' E}{\partial g_I}\frac{\partial\bar{g}}{\partial g_e g_N} - \frac{\partial\triangle' E}{\partial g_e g_N}\frac{\partial\bar{g}}{\partial g_I}\right|}. \tag{C9}$$

We find that deriving the bounds this way reproduces the "naive" bounds obtained from Eq. (13), implying that we can indeed resolve the two measurements via the solution of the coupled equations. Thus, we conclude that the bounds derived from Eq. (13) apply, even when taking the possible variation of the nuclear g factor into account. The treatment for other types of measurements, such as NMR, is less straightforward, and it is not as easily established that we can disentangle them from the HFS measurements. Since this is the case for bismuth, our constraints are only a projection, assuming the above treatment gives the same bounds, i.e., a Zeeman measurement yields the same result as the NMR measurement.